10.2514/6.2019-2057

SAND2019-6077C

Determination of Ballistic Limit of Skin-Stringer Panels Using Nonlinear, Strain-Rate Dependent Peridynamics

Fernando Cuenca[1] and Olaf Weckner[2]
Boeing Commercial Airplanes, Everett, WA, 98204, USA

Stewart A. Silling[3]
Sandia National Laboratories, Albuquerque, NM, 87185, USA

and

Mostafa Rassaian[4]
Boeing Research And Technology, Seattle, WA,98108

Significant testing is required to design and certify primary aircraft structures subject to High Energy Dynamic Impact (HEDI) events; current work under the NASA Advanced Composites Consortium (ACC) HEDI Project seeks to determine the state-of-the-art of dynamic fracture simulations for composite structures in these events. This paper discusses one of three Progressive Damage Analysis (PDA) methods selected for the second phase of the NASA ACC project: peridynamics, through its implementation in EMU. A brief discussion of peridynamic theory is provided, including the effects of nonlinearity and strain rate dependence of the matrix followed by a blind prediction and test-analysis correlation for ballistic impact testing performed for configured skin-stringer panels.

1. Introduction

In this study, we applied a meshless simulation code Emu [1] that is based on the peridynamic theory of solid mechanics. The peridynamic theory is a nonlocal model that uses integro-differential, rather than partial differential, equations in its basic formulation. This approach allows the equations of the peridynamic theory to be applied directly on evolving discontinuities such as growing cracks. Special techniques to model cracks that are sometimes required at the discretized level in finite element codes are not needed in peridynamics, because the equations are compatible with the essential physical nature of cracks as discontinuities in the displacement field. A general discussion of the peridynamic theory can be found in [2].

In the peridynamic theory, each material point x in a continuous body interacts through a nonlocal material model with its neighbors within a cutoff distance δ, which is called the horizon (Figure 1). The interaction between any pair of such neighboring points is called a bond. Bonds carry a force density between the points they connect. The material with a distance δ of x in the initial configuration of the body is called the family of x, denoted $\mathcal{H}$.

[1] Structural Analysis Engineer, Structural Methods And Allowables, 3003 West Casino Road, Everett WA 98204, MC: 03-JP, Member.
[2] Structural Analysis Engineer, Structural Methods And Allowables, 3003 West Casino Road, Everett WA 98204, MC: 03-28, AIAA Senior Member.
[3] Distinguished Member of the Technical Staff, Center for Computing Research, MS-1322, P.O. Box 5800, Sandia National Laboratories, Albuquerque, NM 87185-1322 USA, AIAA Fellow.
[4] Technical Fellow, Structures Technology, 9725 East Marginal Way South, Tukwila, WA 98108, MC: 42-56, AIAA Fellow.

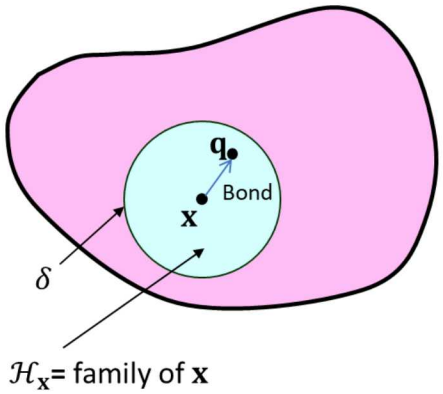

Figure 1. Neighboring points within a cutoff distance of each other interact through bonds.

The equation of motion in the peridynamic theory replaces the divergence of the stress tensor field with an integral as follows:

- Local:

$$\rho\ddot{u}(x,t) = \nabla \cdot \sigma(x,t) + b(x,t).$$

- Peridynamic:

$$\rho\ddot{u}(x,t) = \int_{\mathcal{H}} f(q,x,t)dq + b(x,t)$$

where u is the displacement field, σ is the stress tensor field, b is the prescribed body force density, and f is the bond force density that is supplied by the peridynamic material model and is a function of the deformation. The dimensions of f are force/volume^2. The form of f must always satisfy the following antisymmetry, which ensures that conservation of linear momentum holds globally:

$$f(q,x,t) = -f(x,q,t).$$

There is also a restriction on f arising from conservation of angular momentum; see [2] for details.

A material model associates with each bond in the family of x a value of the bond force density. The bond force density $f(q,x,t)$ can be shown rigorously to be comprised of two parts (Figure 2) that individually arise from the deformations of the families of x and q:

$$f(q,x,t) = T_x(q,x,t) - T_q(x,q,t).$$

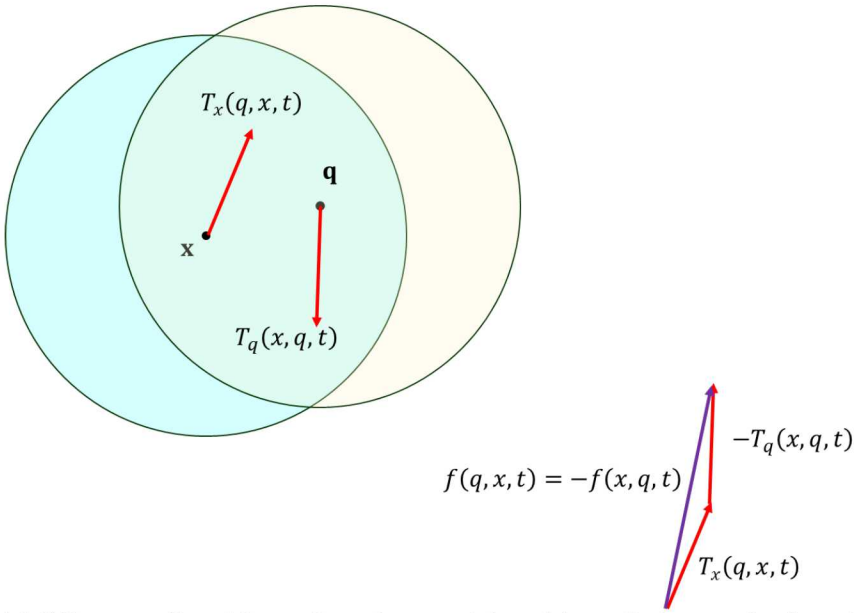

Figure 2. Vectorial difference of bond forces from the material models applied at x and q form the combined bond force density f.

In general, the bond force density contribution $T_x(q,x,t)$ due to the material model at x depends not only on the deformation of the particular bond from x to q, but also on the totality of the deformation of the family $\mathcal{H}$. The mathematical techniques by which this dependence is characterized is the main purpose of state-based material modeling [3], the details of which will be omitted here.

The peridynamic equations lend themselves to a meshless discretization [1] that approximates the integral in the equation of motion by a finite sum over Lagrangian nodes:

$$\int_{\mathcal{H}} f(q,x_i,t)dq \approx \sum_{j\in\mathcal{H}} f(x_j,x_i,t)V_j$$

where V_j is the volume of node j. This discretization method has the advantages of simplicity and the fact that the discretized material model is identical to the continuum material model. In this study, conventional explicit time integration is used:

$$\rho\ddot{u} \approx \frac{1}{\Delta t^2}(u^{n+1} - 2u^n + u^{n-1}).$$

Damage nucleation and progression are modeled through bond breakage, which means that after the deformation of a bond meets some prescribed failure criterion, it breaks irreversibly, after which it no longer carries any force density. When one bond breaks, it changes the force distributions in neighboring bonds, making it more likely that they will break. This leads to progressive failures that, according to the material model and loading conditions, manifest themselves as discrete cracks or distributed damage (Figure 3). In composites, failure occurs as a combination of these two modes.

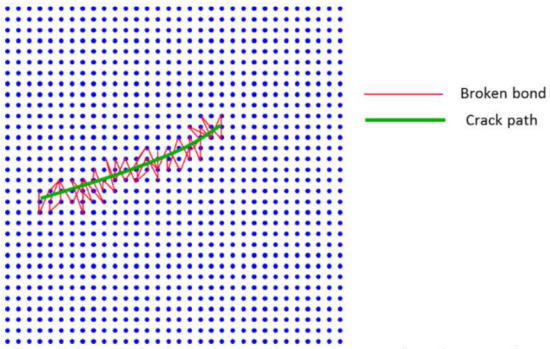

Figure 3. Breakage of peridynamic bonds leads to the nucleation and progression of damage.

Several authors have published peridynamic material models for composites. Among the first was [4], which demonstrated delamination and material failure in carbon-epoxy laminates in three dimensions. Other models for composites include [5,6,7,8,9]. These models all share the same feature that creates strong anisotropy in elastic and damage response: special bonds in the direction of the fiber reinforcement within each lamina have elastic response that is different (usually stiffer and stronger) than all the other bonds. These other bonds represent the response of the matrix material within each lamina and usually the interply response as well.

In the composite material model used in this study, the bond force is given by

$$T^0{}_x(q,x,t) = \begin{cases} C_f \epsilon(q,x,t), & \text{fiber} \\ C_m(\varphi)\epsilon(q,x,t) + k\vartheta, & \text{matrix} \\ C_i \epsilon(q,x,t), & \text{interply} \end{cases}$$

where ϵ is the bond strain, ϑ is the dilatation (volume change) of the family, and $C_f, C_i, C_m(\varphi)$ are material parameters. φ is the angle of the bond in a lamina relative to the fiber direction. These parameters are fitted to the measured elastic constants $E_{11}, E_{22}, \upsilon_{12}, G_{12}, G_{13}, G_{23}, E_{33}$.

In the present study, we are augmenting the material model to include rate-dependent bond response. This rate dependence is included through linearly viscoelastic terms of the form [10,11]

$$T_x(q,x,t) = T^0{}_x(q,x,t) + D\dot{\epsilon}(q,x,t)$$

to the elastic composite material model given above, where D is a constant. This term helps to reproduce the increase in stress observed in Hopkinson bar experiments with laminates under high-rate tensile loading [12]. At constant strain rate, the viscoelastic term shifts the stress-strain curve up or down, as illustrated in Figure 5.

We also incorporated nonlinear softening in the elastic response of matrix bonds given above, so that $C_m(\varphi)$ depends on the bond strain:

$$C_m(\varphi,\epsilon) = \frac{C^0{}_m(\varphi)}{1 + \epsilon/\epsilon_0}$$

where $C^0{}_m(\varphi)$ is the bond stiffness at zero strain, and ϵ_0 is a constant. The net effect is to soften the response of matrix bonds as they extend as illustrated schematically in Figure 4. This term enables the model to more accurate reproduce certain coupon tests such as off-axis tension, as shown in Figure 5.)

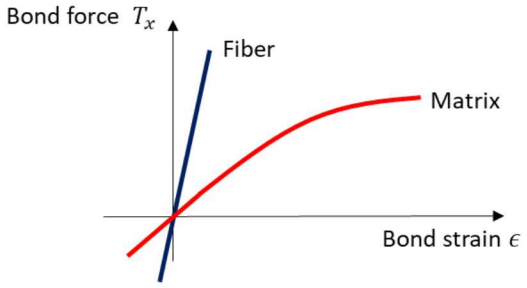

Figure 4. Nonlinear response of matrix bonds (volume-dependent term is not shown).

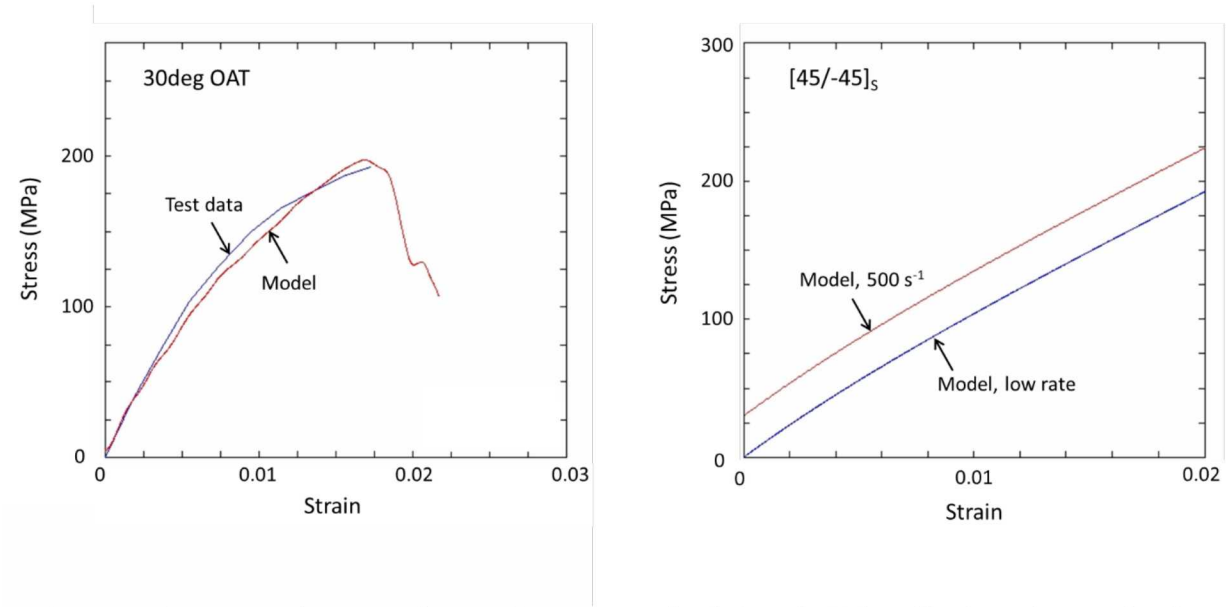

Figure 5. Left: Computed stress-strain curve from an Emu simulation of a 30deg off-axis tension test showing material nonlinearity prior to specimen failure. (Test data from Hyder et al. [13].) Right: Computed stress-strain curves in a laminate for low and high strain rate.

2. Peridynamics Model

Ballistic impact testing was performed on configured skin-stringer panels. The test panel is made of IM7/8552 material system with a ply thickness of 0.0072". The skin is a flat 25"x25" panel with an all tape 25/50/25 quasi-isotropic 24-ply layup and has a nominal thickness of 0.1728". A co-cured hat stringer runs through the center of the panel and has 12 plies in a 33/50/17 all-tape layup, which results in a nominal thickness of 0.0864". The stringer height is 1.4" and it has a total width of about 5.4". The cured configured panel is bolted to the test frame using a picture frame arrangement with 48 bolts around the periphery, see Figure 6 and 7. In the simulation we hold the panel nodes under the test frame fixed.

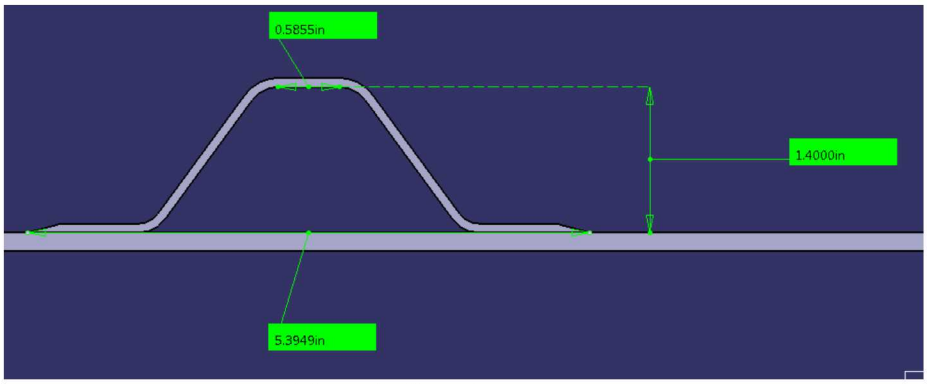

Figure 6. Hat stringer geometry

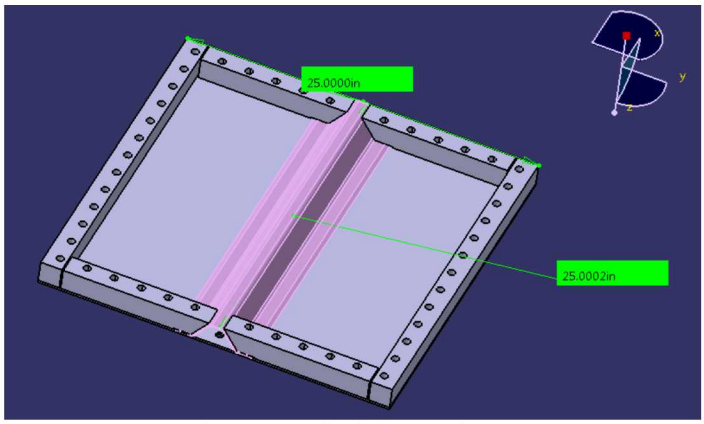

Figure 7. Bolted Frame Fixture

For the peridynamic simulation we smear the 24 skin plies into 8 plies of identical total thickness T and identical A matrix, which characterizes the in-plane plate stiffnesses. This implies that we are also matching the so-called smeared D matrix, $D = T^2/12\ A$, which caracteriszes the plate bending stiffness in thick composites plates. The 12 stringer plies are also smeared into 8 equivalent plies, see Figure 8 below. The noodle is modeled as homogeneous isotropic material with a modulus corresponding to resin. The same fracture toughnesses G1C and G2C for mode 1 and 2 are used between the individual sublamiantes of the skin and stringer, as well as between skin and stringer bondline.

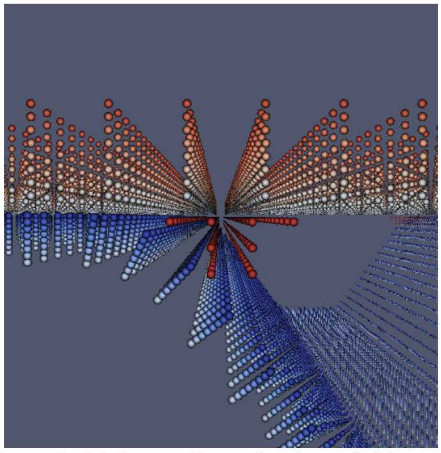
Figure 8. Through thickness discretization of skin-stringer panel

The impactor used is a modified ASTM D.8101 projective made of aluminum 6061 and has a 2.0” diameter. It has a mass of 91 grams (0.2lb) and is shown in Figure 9 together with the panel at the point of initial impact.

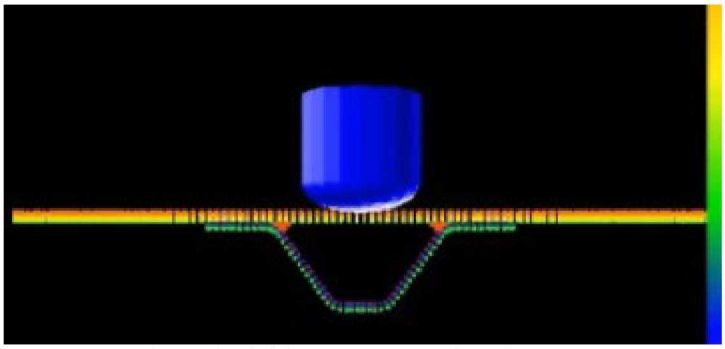
Figure 9 Rigid Impactor at point of contact

Using a uniform in-plane grid spacing of 0.141" the overall model has aobut 130,000 nodes for the composite panel. The peridynamic horizon was chose close to twice the in-plane grid spacing which has proven to be sufficiently large for ballistic limit simulations. During the explicit time integration a constant time step of dt = 1E-7 s was used, together with a safety factor of 0.8.

The composite lamina material model consists of bonds in the fiber and matrix directions. The stiffness of these bonds can be determined as a function of the four in-plane elstic constants E11, E22, G12, ν12 by looking at homogeneous deformations of the lamina. Damage is propagated when these bonds exceed their critical bond strain, which is different in tension and compression. Delaminations are captured through out-of-plane bonds wich are governed by critical shear and normal strains representing mode I and mode II. All material model inputs and their test conditions are listed in Table 1.

Table 1 Peridynamic material model input parameters for IM7/8552

Parameter	Description	Test Conditions	Parameters
□	Density	Scale	98.6 lb/ft^3
E_{11}	Lamina elastic modulus	Uniaxial tension	22.05 Msi
E_{22}	Lamina elastic modulus	Uniaxial tension	1.355 Msi
υ_{12}	Lamina Poisson ratio	Uniaxial tension	0.356
G_{12}	Lamina shear modulus	Shear	0.68 Msi
E_{33}	Transverse elastic modulus	Compression thru thickness	1.355 Msi
G_{13}	Transverse shear modulus	Shear thru thickness	0.68 Msi
e_{fc0}	Fiber failure strain (compression)	Uniaxial compression (0deg)	-0.01229
e_{ft0}	Fiber failure strain (tension)	Uniaxial tension (0deg)	0.01578
e_{mc0}	Matrix failure strain (compression)	Uniaxial compression (90deg)	-0.0294
e_{mt0}	Matrix failure strain (tension)	Uniaxial tension (90deg)	0.00715
e_{ms0}	Matrix failure strain (shear)	Shear (+/- 45deg)	0.01944
G_{IC}	Delamination energy release rate (mode I)	Double Cantilever Beam (DCB)	1.14 in-lbf/in^2
G_{IIc}	Delamination energy release rate (mode II)	End Notch Flexure (ENF)	3.52 in-lbf/in^2

3. Peridynamics Blind Predictions

Before modeling the configured panel we first removed the stringer and ran a simulation to determine the v50 of the unconfigured panel, for which test data is known, see Figure 10. The blue line at 356 ft/s represents the experimental value for the ballistic limit / v50.

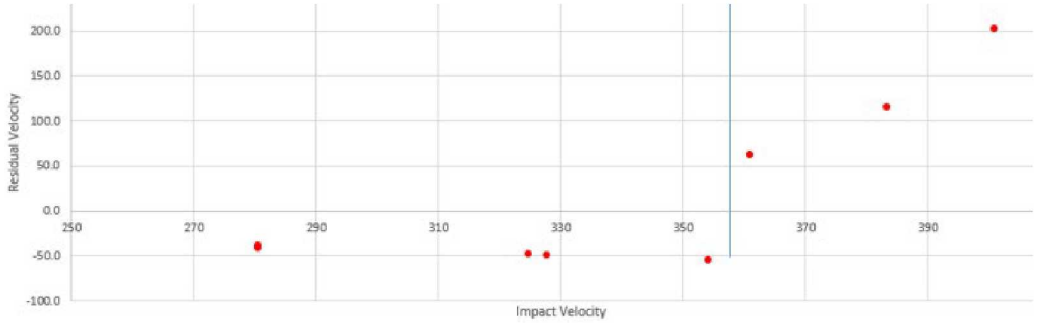

Figure 10 Ballistic limit testing for unconfigured panel

Using the same simulation setup as described in Section 2 we obtain a simulated v50 of 365 ft/s, which is close to the experimental value. Figure 11 shows the time history of the impactor indicating a rebound velocity with only 3% of the initial kinetic energy. Also shown in Figure 11 is the final damage state.

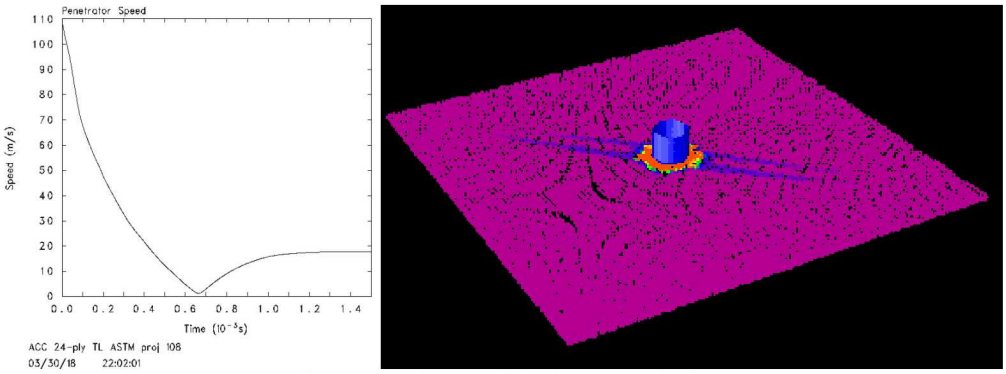

Figure 11 History of the impact velocity

Next we added the stringer into the model and ran two bounding cases at 426 ft/s (rebound, LHS) and 459 ft/s (penetration, RHS), see Figure 12.

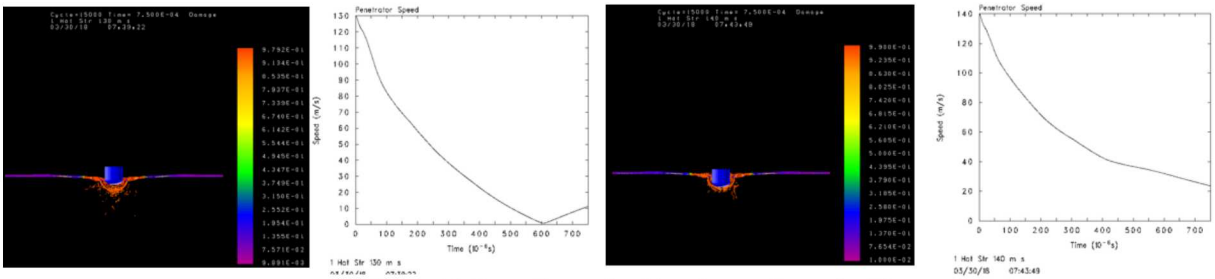

Figure 12 Bounding velocities for configured v50

Based on these results, we predict a v50 velocity of 436 ft/s. Note that this was a blind prediction as the test had not been performed at the time of the prediction. A plot of the delamination damage for the 459 ft/s case is shown in Figure 13.

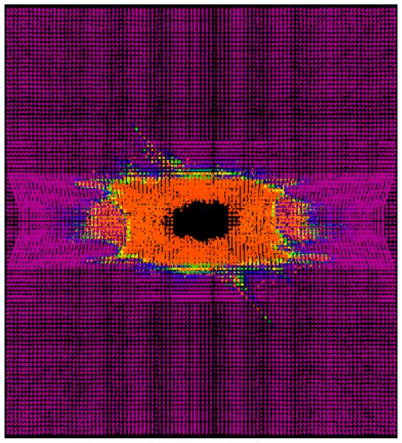

Figure 13 Panel Damage

4. Correlation between blind EMU predictions and test data

The testing shown in Figure 14 results in a v50 = 383 ft/s. The EMU blind prediction was 14% higher at 436 ft/s. The authors consider to be reasonably close, given the uncertainty in some of the input parameters, as well as scatter in the test data. Future improvements may be made by revisiting the through thickness homogenization approach and running a ply-by-ply model.

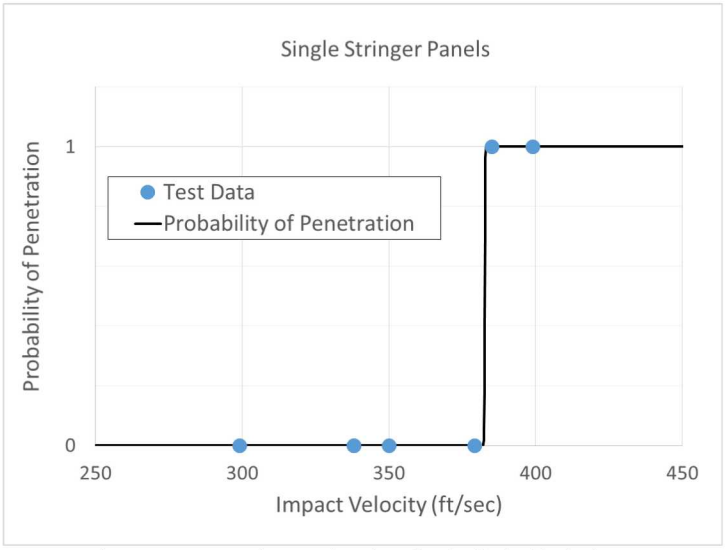

Figure 14 Experimental value for ballstic limit / v50

In terms of the predicted damage state the EMU simulatons resulted damage dimensions along the stringer, and across similar to the ones observed in the NDI testing, see Figure 15.

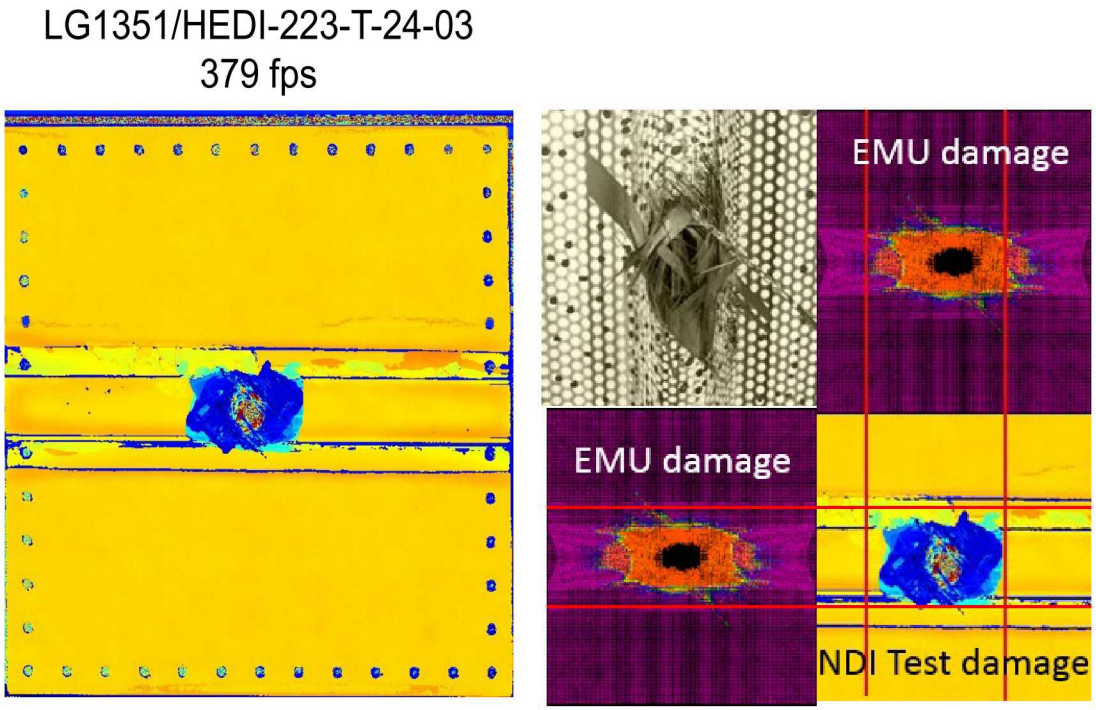

Figure 15 Correlation between NDI damage and predicted damage (EMU)

I. Summary

In this paper we presented peridynamic simulation for high velocity impact events with the goal of determining the ballistic limit, or V_{50} velocity for configured structures. In particular a hat-stringer stiffened composite panel was simulated using a modified ASTM impactor. Building on the unconfigured test for which test data is available a series of analysis to bound the v50 of the configured case were performed. The ballistic limit predicted by the peridynamic approach was 14% higher than the experimental v50 value. The predicted damage size is similar to the NDI test data.

Acknowledgements

The material in this paper is based upon work supported by NASA under Award No. NNL09AA00A. Any opinions, findings, and conclusions or recommendations expressed in this material are those of the author(s) and do not necessarily reflect the views of the National Aeronautics and Space Administration.

Sandia National Laboratories is a multimission laboratory managed and operated by National Technology and Engineering Solutions of Sandia, LLC, a wholly owned subsidiary of Honeywell International, Inc., for the U.S. Department of Energy's National Nuclear Security Administration under contract DE-NA0003525.

References

[1] Silling, S. A., & Askari, E. (2005). A meshfree method based on the peridynamic model of solid mechanics. Computers & structures, 83(17-18), 1526-1535.

[2] Silling, S. A., & Lehoucq, R. B. (2010). Peridynamic theory of solid mechanics. In Advances in applied mechanics (Vol. 44, pp. 73-168). Elsevier.

[3] Silling, S. A., Epton, M., Weckner, O., Xu, J., & Askari, E. (2007). Peridynamic states and constitutive modeling. Journal of Elasticity, 88(2), 151-184.

[4] Xu, J., Askari, A., Weckner, O., & Silling, S. (2008). Peridynamic analysis of impact damage in composite laminates. Journal of Aerospace Engineering, 21(3), 187-194

[5] Hu, W., Ha, Y. D., & Bobaru, F. (2011). Modeling dynamic fracture and damage in a fiber-reinforced composite lamina with peridynamics. International Journal for Multiscale Computational Engineering, 9(6).

[6] Hu, W., Ha, Y. D., & Bobaru, F. (2012). Peridynamic model for dynamic fracture in unidirectional fiber-reinforced composites. Computer Methods in Applied Mechanics and Engineering, 217, 247-261.

[7] Kilic, B., Agwai, A., & Madenci, E. (2009). Peridynamic theory for progressive damage prediction in center-cracked composite laminates. Composite Structures, 90(2), 141-151.

[8] Oterkus, E., & Madenci, E. (2012). Peridynamic analysis of fiber-reinforced composite materials. Journal of Mechanics of Materials and Structures, 7(1), 45-84.

[9] Yu, Y., & Wang, H. (2014). Peridynamic analytical method for progressive damage in notched composite laminates. Composite Structures, 108, 801-810.

[10] Weckner, O., & Mohamed, N. A. N. (2013). Viscoelastic material models in peridynamics. Applied Mathematics and Computation, 219(11), 6039-6043.

[11] Dorduncu, M., Barut, A., & Madenci, E. (2016). Peridynamic truss element for viscoelastic deformation. In 57th AIAA/ASCE/AHS/ASC Structures, Structural Dynamics, and Materials Conference (p. 1721).

[12] Gilat, A., Goldberg, R. K., & Roberts, G. D. (2002). Experimental study of strain-rate-dependent behavior of carbon/epoxy laminates, Composites Science and Technology, 62, 1469-1476.

[13] Hyder, I., Schaefer, J., Justusson, B., Wanthal, S., Leone, F., & Rose, C., (2018). Assessment of intralaminar progressive damage and failure analysis methods using an efficient evaluation framework, https://ntrs.nasa.gov/search.jsp?R=20170010326 2018-02-02T16:05:54+00:00Z